*Journal of Sound and Vibration* (2002) **253**(3), 603–630
doi:10.1006/jsvi.2001.4066, available online at http://www.idealibrary.com on IDEAL®

# A FINITE ELEMENT FORMULATION FOR COUPLING RIGID AND FLEXIBLE BODY DYNAMICS OF ROTATING BEAMS

K. HU AND N. VLAHOPOULOS

*Department of Naval Architecture and Marine Engineering, The University of Michigan, 2600 Draper Road, Ann Arbor, MI 48109-2145, U.S.A.*

AND

Z. P. MOURELATOS

*Vehicle Analysis & Dynamics Lab, Research & Development Center, General Motors Corporation, 30500 Mound Road 106, Box 9055, Warren, MI 48090-9055, U.S.A.*

(*Received* 10 *April* 2001, *and in final form* 29 *October* 2001)

The work presented in this paper is based on an existing comprehensive formulation for rotating flexible systems. In the existing formulation the flexible degrees of freedom (d.o.f.) are represented by an analytically computed modal basis and the coupling matrices between the rigid- and the flexible-body d.o.f. are developed based on the analytical modal representation of the flexible d.o.f. In this paper, the existing formulation is generalized for rotating beams by representing the flexible d.o.f. either as physical d.o.f. of a finite element formulation or as a set of retained and internal d.o.f. of a Craig–Bampton formulation. The coupling matrices between the rigid-body rotation and the flexible d.o.f. are developed accordingly. The non-linear effects from the work done by the centrifugal forces are included in the formulation. Finite element shape functions of a beam element in a three-dimensional space and finite element shape functions for solid elements are employed for deriving the coupling terms between the rigid-body d.o.f. and the physical d.o.f. An additional transformation is required and performed when the right-body d.o.f. are coupled with the internal and the retained d.o.f. of a Craig–Bampton formulation. The coupled system of equations is solved in the time domain by combining the Newmark method for time integration and the Newton–Raphson method for solving the non-linear system of equations within each time step. Analyses are performed for a flexible rotating beam in order to validate the development. An analytical solution is compared with the new formulations that represent the rotating beam flexibility with the physical d.o.f. of beam or solid elements. The analytical solution is also compared to the formulation that represents the flexible d.o.f. in terms of retained and internal d.o.f. of a Craig–Bampton formulation. Very good correlation between the analytical and numerical results is observed. 

## 1. INTRODUCTION

Coupling right- and flexible-body dynamics of rotating structures has been discussed in the literature extensively, and an overview of previous works will be presented first. Several papers have been presented in the past for modelling the combined rigid- and flexible-body dynamics of beams. A comprehensive theory that allows to compute small vibrations of a general rotating beam subjected to prescribed base excitation was presented [1]. A varying cross-section and material properties were considered for the beam. The effects of

0022-460X/02/$35.00 

centrifugal stiffening and of the vibration induced by Coriolis forces were included in the formulation. A radially rotating flexible beam fixed to a rigid body was analyzed [2]. A set of fully coupled non-linear equations of motion were derived using the extended Hamilton principle. The effect of the coupling terms between rigid-body and flexural motion on the vibration was investigated. It was identified that for small values of the ratio between the flexible rigidity of the beam and the rigid inertia of the beam the uncoupled equations led to substantially incorrect results. A computational procedure for multi-body dynamics analysis based on a finite deformation beam model was presented [3]. The beam formulation was based on fully non-linear strain measures that remain invariant with respect to the rigid-body motions. An inertial reference system was used for the beam dynamics, and the flexible degrees of freedom (d.o.f.) were computed with respect to a convected reference frame that rotates with the beam components. The development was targeting computations of the dynamics of flexible beams that undergo a variety of structural deformations in addition to large overall motions. The free flexural vibrations of a spinning, finite Timoshenko beam for the six classical boundary conditions were solved analytically in reference [4]. Expressions for the mode shapes and the natural frequencies were derived. A flexible-body dynamic formulation, called the augmented imbedded geometric approach, was developed for beam structures undergoing large overall motion in a two-dimensional space [5]. The elastic deformation was characterized as a superposition of a number of assumed global shape functions. Problems with cantilevered or pinned–pinned conditions were addressed. A formulation based entirely on the energy principle was presented in reference [6] for dynamic analysis of a planar Timoshenko's beam with finite rotations. An inertial and a rotating frame were introduced in order to simplify the computational process. The kinetic energy was obtained in the inertial frame, while the rotating frame was utilized for deriving the strain energy under a small strain assumption. The resulting equations of motion were defined in terms of a fixed global co-ordinate system. A systematic development for the non-linear dynamics of multi-body systems in planar motion was presented in reference [7] based on the two-dimensional beam theory. A simple quadratic form for the kinetic energy and a spatial form of the strain which simplifies the strain energy expression were derived. A time stepping scheme appropriate for multi-body systems with large difference in their relative stiffness was also developed.

Formulations for modelling the rigid- and flexible-body dynamics of general objects have also been presented. A method of quadratic components was developed in reference [8] for analyzing rotating flexible structures using a system of non-linearly coupled deformation modes. The formulation utilizes a non-linear configuration space in which all the kinematic constraints are satisfied up to the second order. The effects of rotary inertia on the extensional tensile force and on the eigenvalues of beams rotating about the transverse axis were presented in reference [9]. A method for dynamic simulation of multi-body systems that include large-scale finite element models of flexible bodies was presented in reference [10]. An optimal lumped inertia technique was developed in order to avoid computation of the coupling matrices between the right-body d.o.f. and the flexible d.o.f. in the finite element representation of the flexible bodies. Inertia was lumped optimally at a subset of nodes of the finite element model, thus, simplifying the evaluation of the coupling terms in the equations of motion.

The work presented in this paper is based on a previous formulation that couples rigid- and flexible-body dynamics for rotating beams [11–13]. In the existing formulations, the equations of motion were derived using a non-linear formulation that retains second order terms in the strain–displacement relationship. Thus, the effect of all the geometric elastic non-linearities on the bending displacement was accounted for, without the need to include

the high-frequency axial modes of vibration [11]. A Lagrangian formulation was employed for deriving the dynamic equations for a rotating beam [12, 13]. In the previous work of references [11–13] the flexible d.o.f. were expressed in terms of the analytically derived modal basis for a beam. The coupling matrices between flexible d.o.f. and the rigid-body d.o.f. were developed in terms of the analytically evaluated modes of a beam. The new developments presented in this paper are: (1) The flexible d.o.f. are represented as physical d.o.f. of a finite element formulation in the rigid- and flexible-body dynamics algorithm. Beam finite elements in a three-dimensional space or three-dimensional solid finite elements are utilized to represent the flexible d.o.f. (2) The shape functions of the beam finite elements and the shape functions of the solid finite elements are employed for deriving the coupling terms between the rigid-body d.o.f. and the flexible d.o.f. (3) As an alternative, the flexible d.o.f. of the rigid- and flexible-body dynamics algorithm are represented as internal and retained d.o.f. of a Craig–Bampton finite element based formulation [14]. (4) The coupling terms between the rigid-body d.o.f. and the flexible d.o.f. are derived based on the Craig–Bampton representation of the flexible d.o.f. The shape functions of the finite elements used in the Craig–Bampton formulation are employed in the development of the coupling terms. A transformation is also incorporated in the development of the coupling terms in order to account for the relationship between the physical finite element d.o.f. and the internal and retained d.o.f. of the Craig–Bampton formulation. (5) Development of numerical solutions that can handle the representation of the flexible d.o.f. in the coupled rigid–flexible body dynamics algorithm as finite element d.o.f. or as internal and retained d.o.f. of a Craig–Bampton formulation. (6) A comprehensive validation of the new methodology is presented based on a rotating flexible beam for which an analytical solution is calculated and utilized as a reference [15].

Results computed by the three alternative forms of the new formulation are presented. The flexible d.o.f. are presented either as physical d.o.f. of beam elements in a three-dimensional space or as physical d.o.f. of three-dimensional solid elements or as Craig–Bampton d.o.f. derived from a three-dimensional solid finite element model. Excellent correlation with the analytical results is observed for all three cases.

## 2. MATHEMATICAL FORMULATION

### 2.1. EQUATIONS OF MOTION

The theoretical background for deriving the equations of motion will be overviewed first. The equations of motion employed in this work originate from references [11–13, 16]. The right-body rotation is coupled with the flexible deformation of a deformable body by utilizing a floating frame of reference [16]. In a floating frame of reference, the motion of any point on a body is defined as the motion of the body reference with respect to a global co-ordinate system plus the motion of the material point on the body with respect to the body reference, as shown in Figure 1; therefore, the location of any point $P$ on the body can be described as vector $\{r\}$ in the global system:

$$\{r\} = \{R\} + [A]\{u\} = \{R\} + [A](\{u_0\} + \{u_f\}), \tag{1}$$

where $\{R\}$ is the global position vector of the origin of the body co-ordinate system, $[A]$ is the transformation matrix between the global and the body system, and $\{u\} = \{u_0\} + \{u_f\}$ is the location vector in the body system, where $\{u_0\}$ is the position vector of $P$ at its undeformed state, and $\{u_f\}$ is the elastic deformation of $P$.

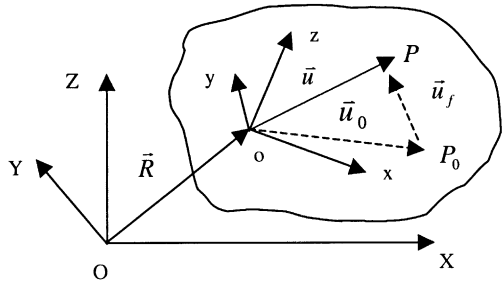


Figure 1. Global co-ordinate system $XYZ$ and body co-ordinate system $xyz$.

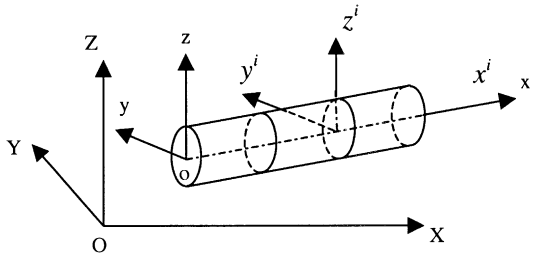


Figure 2. Three different co-ordinate systems: global co-ordinate system $XYZ$, body co-ordinate system $xyz$, element co-ordinate system $x^i y^i z^i$.

When the finite element method is used, the element co-ordinate systems must be introduced. The global co-ordinate system, the body co-ordinate system and an element co-ordinate system are depicted in Figure 2. It has been proved that the conventional shape functions of a beam element can describe an arbitrary rigid-body translation; however, they cannot describe an arbitrary rigid-body rotation. Therefore, the body system has to be chosen in such a way that it is initially parallel to the element co-ordinate system, otherwise an intermediate element co-ordinate system has to be introduced [16]. The situation is similar when solid finite elements are used. Since the shape functions of a solid element can describe an arbitrary rigid-body motion, there is no need to introduce the intermediate element co-ordinate system, even though the body co-ordinate system is not initially parallel to the element system. Therefore, for both beam finite elements and solid finite elements the position vector and the elastic deformation within an element can be expressed in terms of the nodal values as

$$\{u_0\} = [N]\{e_0\} \quad \text{and} \quad \{u_f\} = [N]\{e_f\}, \tag{2}$$

where $[N]$ is the matrix containing the shape functions of either a three-dimensional beam finite element or a solid finite element, $\{e_0\}$ the vector containing the components of each nodal d.o.f. in the undeformed state, and $\{e_f\}$ the vector containing the components of the flexible d.o.f. at the node of an element. The overall deformation $\{e\}$ at the element nodes can be written in terms of the undeformed state and the flexible deformation:

$$\{e\} = \{e_0\} + \{e_f\}. \tag{3}$$

By taking into account equations (2) and (3), equation (1) can be written as

$$\{r\} = \{R\} + [A][N]\{e\}. \tag{4}$$

Considering only rotation along a constant axis in space as a rigid-body motion, the global position vector $\{R\}$ is a constant vector. The velocity vector can be derived by differentiating equation (4) with respect to time, i.e.,

$$\{\dot{r}\} = [A_\theta][N]\{e\}\dot{\theta} + [A][N]\{\dot{e}_f\}, \tag{5}$$

where $[A_\theta]$ is the derivative of the transformation matrix $[A]$ with respect to the angle of rotation $\theta$. In the derivation of equation (5), it has been considered that the position of the origin of the body co-ordinate system and the undeformed position in the body co-ordinate system do not change with time, i.e., $\{\dot{R}\} = \{0\}$ and $\{\dot{e}_0\} = \{0\}$.

The velocity vector of equation (5) can be used to calculate the kinetic energy as

$$KE = \frac{1}{2}\int_V \rho\{\dot{r}\}^{\mathrm{T}}\{\dot{r}\}\,\mathrm{d}V, \tag{6}$$

where $\rho$ is the mass density per unit volume. The mass matrix for a finite element contains both inertia terms and coupling terms between rigid-body and flexible d.o.f., and can be derived from the kinetic energy of equation (6) as

$$[M^e] = \int_{V^e} \rho \begin{bmatrix} \{e\}^{\mathrm{T}}[N]^{\mathrm{T}}[A_\theta]^{\mathrm{T}}[A_\theta][N]\{e\} & \{e\}^{\mathrm{T}}[N]^{\mathrm{T}}[A_\theta]^{\mathrm{T}}[A][N] \\ sym & [N]^{\mathrm{T}}[N] \end{bmatrix} \mathrm{d}V$$

$$= \begin{bmatrix} M^e_{\theta\theta} & \{M^e_{\theta f}\} \\ sym & [M^e_{ff}] \end{bmatrix}, \tag{7}$$

where $V^e$ is the volume of an element, $[M^e_{ff}]$ the mass matrix associated with the flexible d.o.f., $M^e_{\theta\theta}$ the inertia associated with the rigid-body rotation, and $\{M^e_{\theta f}\}$ the row vector that couples the rigid-body rotation and the flexible d.o.f. Superscript "$e$" indicates an element level quantity. The terms of the mass matrix are expressed as

$$M^e_{\theta\theta} = \{e\}^{\mathrm{T}}[T^e]\{e\}, \quad \{M^e_{\theta f}\} = \{e\}^{\mathrm{T}}[H^e], \quad [M^e_{ff}] = \int_{V^e} \rho[N]^{\mathrm{T}}[N]\,\mathrm{d}V, \tag{8}$$

where

$$[T^e] = \int_{V^e} \rho[N]^{\mathrm{T}}[A_\theta]^{\mathrm{T}}[A_\theta][N]\,\mathrm{d}V \text{ and } [H^e] = \int_{V^e} \rho[N]^{\mathrm{T}}[A_\theta]^{\mathrm{T}}[A][N]\,\mathrm{d}V.$$

Matrix $[M^e_{ff}]$ is identical to the conventional consistent finite element mass matrix. The mass matrix of equation (7) can be employed in the expression for the kinetic energy. Then, Lagrange's equation is used to derive the following equations of motion in matrix form:

$$\begin{bmatrix} M_{\theta\theta} & \{M_{\theta f}\} \\ sym & [M_{ff}] \end{bmatrix} \begin{Bmatrix} \ddot{\theta} \\ \{\ddot{e}_f\} \end{Bmatrix} + \begin{bmatrix} 0 & 0 \\ 0 & [C_{ff}] \end{bmatrix} \begin{Bmatrix} \dot{\theta} \\ \{\dot{e}_f\} \end{Bmatrix} + \begin{bmatrix} 0 & 0 \\ 0 & [K_{ff}] \end{bmatrix} \begin{Bmatrix} \theta \\ \{e_f\} \end{Bmatrix} = \{Q_v\} + \{Q_e\}, \tag{9}$$

where $\theta$ is the rigid-body rotation, $\{e_f\}$ is the flexible d.o.f., and $[C_{ff}]$ and $[K_{ff}]$ are the finite element damping and stiffness matrices, respectively, $\{Q_v\}$ is the quadratic velocity vector that contains the effect of the centrifugal force and Coriolis force, and $\{Q_e\}$ is the vector of generalized external forces. In equation (9) all the terms are expressed with respect to the global co-ordinate system and they are derived from assembling the corresponding element quantities. The quadratic velocity vector for a finite element is

$$\{Q_v^e\} = \begin{Bmatrix} -2\{e\}^{\mathrm{T}}[T^e]\{\dot{e}_f\}\dot{\theta} \\ [T^e]\{e\}\dot{\theta}^2 + 2[H^e]\{\dot{e}_f\}\dot{\theta} \end{Bmatrix}. \tag{10}$$

The $[T^e]\{e\}\dot{\theta}^2$ and $2[H^e]\{\dot{e}_f\}\dot{\theta}$ terms represent the centrifugal and coriolis forces respectively.

The vector of generalized forces can be obtained by considering the virtual work done by all forces acting on the body. For the externally applied forces the virtual work is

$$\delta W_{ee} = \{Q_{ee}\}^{\mathrm{T}}\{\delta q\}, \tag{11}$$

where $\{Q_{ee}\}$ is the vector of external forces, $\{\delta q\} = \left\{\begin{smallmatrix}\delta\theta \\ \{\delta e_f\}\end{smallmatrix}\right\}$ the vector of virtual displacements, and $\delta W_{ee}$ the virtual work done by the external forces. The vector of the external forces is

$$\{Q_{ee}\} = \begin{Bmatrix} \{e\}^{\mathrm{T}}[N]^{\mathrm{T}}[A_\theta]^{\mathrm{T}}[A]\{F\} \\ [N]^{\mathrm{T}}\{F\} \end{Bmatrix}, \tag{12}$$

where $\{F\}$ is the vector including the externally applied forces on each physical d.o.f. of the finite element formulation. The non-linear effect of the work done by the centrifugal forces must be also taken into account [12, 15]. It can be derived by accounting for the work done by the centrifugal force due to a virtual displacement imposed on the flexible d.o.f. If the rotation axis is perpendicular to the longitudinal axis of the rotating member, the corresponding generalized force vector becomes

$$\{Q_{ec}\} = \begin{Bmatrix} 0 \\ -[[T_2] + [T_3]]\{e_f\} \end{Bmatrix}, \tag{13}$$

where $[T_2]$ and $[T_3]$ are matrices associated with the effect of the centrifugal forces in the two bending planes. The derivation of $[T_2]$ and $[T_3]$ depends on the type of shape functions utilized in the finite element formulation. Based on equations (12) and (13) the generalized force vector becomes

$$\{Q_e\} = \begin{Bmatrix} \{e\}^{\mathrm{T}}[N]^{\mathrm{T}}[A_\theta]^{\mathrm{T}}[A]\{F\} \\ [N]^{\mathrm{T}}\{F\} - [[T_2] + [T_3]]\{e_f\} \end{Bmatrix}. \tag{14}$$

This concludes the review of the rigid- and flexible-body formulation utilized in this work. In the following sections the new developments associated with the representation of the flexible d.o.f. as physical d.o.f. of a finite element formulation or as d.o.f. of a Craig–Bampton formulation are presented.

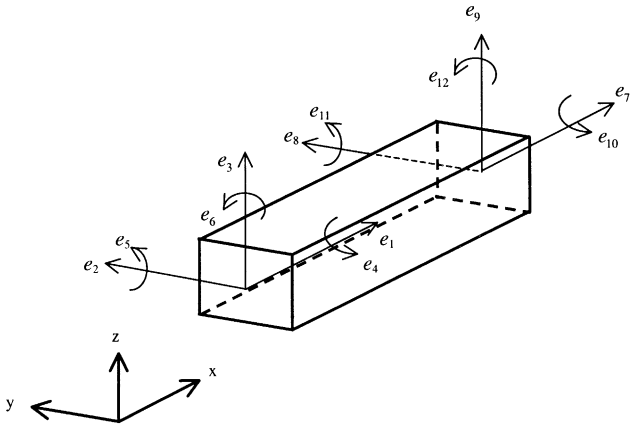


Figure 3. A 3D beam element with 12 degrees of freedom.

## 2.2. THREE-DIMENSIONAL BEAM ELEMENT FORMULATION

Figure 3 depicts the d.o.f. associated with the nodes of a beam element in a three-dimensional space. The shape function matrix for the element is [17]

$$[N] = \begin{bmatrix} 1-r & 0 & 0 & 0 & 0 & 0 & r & 0 & 0 & 0 & 0 & 0 \\ 0 & 1-3r^2+2r^3 & 0 & 0 & 0 & (r-2r^2+r^3)l & 0 & 3r^2-2r^3 & 0 & 0 & 0 & (r^3-r^2)l \\ 0 & 0 & 1-3r^2+2r^3 & 0 & -(r-2r^2+r^3)l & 0 & 0 & 0 & 3r^2-2r^3 & 0 & (r^2-r^3)l & 0 \end{bmatrix}_{3\times 12}$$

$$= \begin{bmatrix} \{S_1\} \\ \{S_2\} \\ \{S_3\} \end{bmatrix}, \tag{15}$$

where $r = (x - x_0)/l$ is the local relative co-ordinate, $x$ is the co-ordinate of any point along the beam axis in the body co-ordinate system, $x_0$ is the co-ordinate of the first element node, $l$ is the length of the element, and $\{S_1\}$, $\{S_2\}$, $\{S_3\}$ are the three row vectors of the shape function matrix of equation (15). The $\{S_1\}$ vector is associated with the longitudinal motion while the $\{S_2\}$ and $\{S_3\}$ vectors represent the two out-of-plane bending motions respectively. The three displacements and three rotations at each of the two nodes of a beam element comprise the 12 d.o.f. of each element.

In this development, the rigid body is considered to be rotating along an axis perpendicular to the longitudinal direction of the beam (rotation around the $Z$-axis is considered, as shown in Figure 4). Thus, the transformation matrix between the global and the body co-ordinate systems becomes

$$[A] = \begin{bmatrix} \cos\theta & -\sin\theta & 0 \\ \sin\theta & \cos\theta & 0 \\ 0 & 0 & 1 \end{bmatrix}. \tag{16}$$

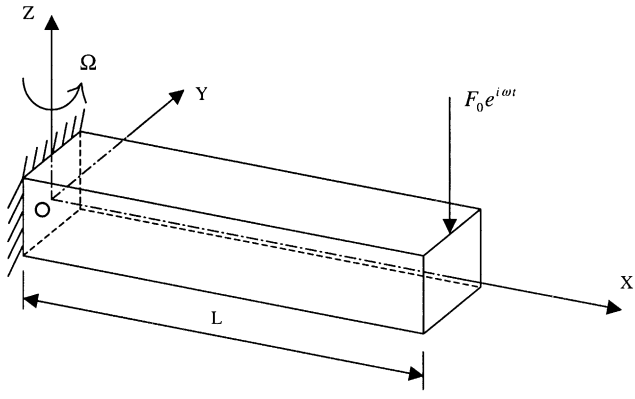


Figure 4. A rotating cantilever beam model.

The derivative of the transformation matrix with respect to the rigid-body rotation is

$$[A_\theta] = \frac{\mathrm{d}[A]}{\mathrm{d}\theta} = \begin{bmatrix} -\sin\theta & -\cos\theta & 0 \\ \cos\theta & -\sin\theta & 0 \\ 0 & 0 & 0 \end{bmatrix}. \tag{17}$$

Due to the selection of the $Z$-axis for the rigid-body rotation, the following relationships hold:

$$[A_\theta^{\mathrm{T}}][A_\theta] = \begin{bmatrix} 1 & 0 & 0 \\ 0 & 1 & 0 \\ 0 & 0 & 0 \end{bmatrix} \quad \text{and} \quad [A_\theta^{\mathrm{T}}][A] = \begin{bmatrix} 0 & 1 & 0 \\ -1 & 0 & 0 \\ 0 & 0 & 0 \end{bmatrix}. \tag{18}$$

Based on the definition of the shape functions matrix $[N]$ for a beam element in a three-dimensional space (equation (15)), the definitions for the element matrices $[T^e]$ and $[H^e]$ (equation (8)) are presented in Appendix A.

The derivation of the matrices associated with the effect of the centrifugal forces on the bending deformations also requires the finite element shape functions. By considering a cantilever beam rotating along an axis perpendicular to the longitudinal direction of the beam, the virtual work done by the centrifugal force $P_x$ due to the bending deformation is [15]

$$\delta W_{ec} = -\int_0^L P_x\left(\frac{\partial v}{\partial x}\right)\delta\left(\frac{\partial v}{\partial x}\right)\mathrm{d}x - \int_0^L P_x\left(\frac{\partial w}{\partial x}\right)\delta\left(\frac{\partial w}{\partial x}\right)\mathrm{d}x, \tag{19}$$

where $\delta W_{ec}$ is the virtual work done by the centrifugal forces due to bending deformation, $v$ and $w$ are the bending displacements in the $y$ and $z$ directions, respectively, and $L$ is the length of the beam. The centrifugal force at any longitudinal position $\xi$ is

$$P_x = \int_{\xi=x}^{L} \rho\Omega^2 a(\xi)\xi\,\mathrm{d}\xi, \tag{20}$$

where $a(\xi)$ is the cross-sectional area of the beam and $\Omega$ is the rotational speed.

In the special case of a uniform beam, $a(\xi)$ and $\rho$ are constant, and the centrifugal force becomes

$$P_x = \tfrac{1}{2}\rho a\Omega^2(L^2 - x^2). \tag{21}$$

The corresponding virtual work associated with a particular finite element can be stated as

$$\delta W_{ce}^e = -\int_{x_0}^{l+x_0} P_x\{e_f\}^{\mathrm{T}} \frac{\mathrm{d}\{S_2\}^{\mathrm{T}}}{\mathrm{d}x}\frac{\mathrm{d}\{S_2\}}{\mathrm{d}x}\{\delta e_f\}\,\mathrm{d}x - \int_{x_0}^{l+x_0} P_x\{e_f\}^{\mathrm{T}} \frac{\mathrm{d}\{S_3\}^{\mathrm{T}}}{\mathrm{d}x}\frac{\mathrm{d}\{S_3\}}{\mathrm{d}x}\{\delta e_f\}\,\mathrm{d}x, \tag{22}$$

where $x_0$ is the longitudinal co-ordinate of the first node of the finite element, $l$ is the length of the finite element, $\{S_2\}$ and $\{S_3\}$ are the row vectors containing the second and third row of the shape functions matrix (equation (15)). The $[T_2]$ and $[T_3]$ matrices (see equation (13)) associated with the effect of the centrifugal forces in the two bending planes will be

$$[T_2^e] = \int_{x_0}^{l+x_0} P_x \frac{\mathrm{d}\{S_2\}^{\mathrm{T}}}{\mathrm{d}x}\frac{\mathrm{d}\{S_2\}}{\mathrm{d}x}\mathrm{d}x \quad \text{and} \quad [T_3^e] = \int_{x_0}^{l+x_0} P_x \frac{\mathrm{d}\{S_3\}^{\mathrm{T}}}{\mathrm{d}x}\frac{\mathrm{d}\{S_3\}}{\mathrm{d}x}\mathrm{d}x. \tag{23}$$

Matrices $[T_2^e]$ and $[T_3^e]$ are evaluated explicitly for three-dimensional beam elements based on the shape functions (equation (15)) and are presented in Appendix A.

### 2.3. THREE-DIMENSIONAL SOLID FINITE ELEMENT FORMULATION

The shape functions matrix for a solid hexahedron element in a three-dimensional space is [18, 19]

$$[N] = \begin{bmatrix} N_1 & 0 & 0 & N_2 & 0 & 0 & \cdots & N_8 & 0 & 0 \\ 0 & N_1 & 0 & 0 & N_2 & 0 & \cdots & 0 & N_8 & 0 \\ 0 & 0 & N_1 & 0 & 0 & N_2 & \cdots & 0 & 0 & N_8 \end{bmatrix}_{3\times 24} = \begin{bmatrix} \{S_1\} \\ \{S_2\} \\ \{S_3\} \end{bmatrix}, \tag{24}$$

where $\{S_1\}$, $\{S_2\}$, and $\{S_3\}$ are row vectors associated with the $x$, $y$, and $z$ directions respectively. The shape functions $N_1$–$N_8$ are defined as [19]

$$\begin{aligned} N_1 &= \tfrac{1}{8}(1-r)(1-s)(1-t), & N_2 &= \tfrac{1}{8}(1+r)(1-s)(1-t), \\ N_3 &= \tfrac{1}{8}(1+r)(1+s)(1-t), & N_4 &= \tfrac{1}{8}(1-r)(1+s)(1-t), \\ N_5 &= \tfrac{1}{8}(1-r)(1-s)(1+t), & N_6 &= \tfrac{1}{8}(1+r)(1-s)(1+t), \\ N_7 &= \tfrac{1}{8}(1+r)(1+s)(1+t), & N_8 &= \tfrac{1}{8}(1-r)(1+s)(1+t). \end{aligned} \tag{25}$$

The translational displacements at each of the eight element nodes constitute the element d.o.f. Similar shape function matrices are considered for solid elements with four sides (tetrahedron) and five sides (pentahedron).

The expression provided in equation (8) for the components of the overall mass matrix remains the same. The appropriate expression of the shape functions matrix $[N]$ for solid elements (equation (24)) is used in the derivation of $[T^e]$ and $[H^e]$. Similarly, the expressions provided in equation (22) with the appropriate modification in the shape functions can be

utilized for computing $[T_2^e]$ and $[T_3^e]$. The $[T^e]$, $[H^e]$, $[T_2^e]$, and $[T_3^e]$ matrices are evaluated numerically using an $n$th point Gaussian integration scheme. The corresponding expressions are presented in Appendix B. The assembly of the global matrices is performed after the element matrices have been computed.

### 2.4. COMPONENT MODE SYNTHESIS (CMS) FORMULATION

The flexible d.o.f. are represented as d.o.f. of a Craig–Bampton method [14] in the coupled rigid- and flexible-body dynamics algorithm. The Craig–Bampton-based formulation utilizes the 3-D solid finite elements of section 2.3. The Craig–Bampton method is used in this work due to its computational efficiency and superior accuracy for representing the flexible-body dynamics. The coupling matrices between the rigid-body and the Craig–Bampton d.o.f. are developed. The flexible d.o.f. are partitioned into internal and retained d.o.f. (superscripts "$i$" and "$r$" respectively). The flexible-body stiffness and mass matrices are partitioned accordingly as

$$[K_{ff}] = \begin{bmatrix} [K_{ff}^{ii}] & [K_{ff}^{ir}] \\ [K_{ff}^{ri}] & [K_{ff}^{rr}] \end{bmatrix}, \quad [M_{ff}] = \begin{bmatrix} [M_{ff}^{ii}] & [M_{ff}^{ir}] \\ [M_{ff}^{ri}] & [M_{ff}^{rr}] \end{bmatrix}. \tag{26}$$

By considering all the retained d.o.f. to be fixed the following eigenvalue problem is solved for the eigenvalues $\omega_j^2$ and the corresponding fixed-interface eigenvectors

$$\{x_j\}, \quad j = 1, 2, \ldots, J, \qquad [[K_{ff}^{ii}] - \omega^2 [M_{ff}^{ii}]]\,\{X\} = \{0\}. \tag{27}$$

The modal and the diagonal matrices containing the eigenvalues are defined as

$$[X] = [\{x_1\} \quad \{x_2\} \cdots \{x_J\}], \qquad [\omega^2] = \begin{bmatrix} \omega_1^2 & & & 0 \\ & \omega_2^2 & & \\ & & \ddots & \\ 0 & & & \omega_J^2 \end{bmatrix}, \tag{28}$$

where $J$ is the total number of computed normal modes in the modal basis. Usually, $J$ is much smaller than the number of internal d.o.f. in equation (27). A set of static (or constraint) modes is also considered in order to compensate for the non-zero values that the retained d.o.f. acquire:

$$\{e_f^i\} = -[K_{ff}^{ii}]^{-1}[K_{ff}^{ir}]\{e_f^r\} = [Y]\{e_f^r\}, \tag{29}$$

where $[Y] = -[K_{ff}^{ii}]^{-1}[K_{ff}^{ir}]$. The internal d.o.f. can be expressed as a linear superposition of the fixed-interface normal modes (equation (28)) and the static modes (equation (29)):

$$\{e_f^i\} = \sum_{j=1}^{j} \alpha_j \{X_j\} + [Y]\{e_f^r\}, \tag{30}$$

where $\alpha_j$ is the modal participation factor of the $j$th fixed-interface mode.

Based on equation (30), the vector of the physical d.o.f. can be expressed as

$$\{e_f\} = \begin{Bmatrix} \{e_f^i\} \\ \{e_f^r\} \end{Bmatrix} = \begin{bmatrix} [X] & [Y] \\ [0] & [I] \end{bmatrix} \begin{Bmatrix} \{\alpha\} \\ \{e_f^r\} \end{Bmatrix}, \tag{31}$$

where $\{\alpha\}$ is the vector of modal participation factors. The flexible physical d.o.f. are replaced by the modal d.o.f. of the fixed-interface modes and the physical retained d.o.f. Thus, the coupled rigid–flexible body dynamics formulation must reflect the set of d.o.f. employed by the Craig–Bampton formulation. The vector of the single rigid d.o.f. and the flexible d.o.f. becomes

$$\begin{Bmatrix} \theta \\ \{e_f\} \end{Bmatrix} = \begin{bmatrix} 1 & \{0\} & \{0\} \\ \{0\} & [X] & [Y] \\ \{0\} & [0] & [I] \end{bmatrix} \begin{Bmatrix} \theta \\ \{\alpha\} \\ \{e_f^r\} \end{Bmatrix} = [\bar{\Phi}] \begin{Bmatrix} \theta \\ [\alpha] \\ [e_f^r] \end{Bmatrix} = [\bar{\Phi}] \begin{Bmatrix} \theta \\ \{\eta\} \end{Bmatrix}, \tag{32}$$

where

$$\{\eta\} = \begin{Bmatrix} \{\alpha\} \\ \{e_f^r\} \end{Bmatrix}, \quad [\bar{\Phi}] = \begin{bmatrix} 1 & \{0\} \\ \{0\} & [\phi] \end{bmatrix} = \begin{bmatrix} 1 & \{0\} & \{0\} \\ \{0\} & [X] & [Y] \\ \{0\} & [0] & [I] \end{bmatrix} \quad \text{and} \quad [\phi] = \begin{bmatrix} [X] & [Y] \\ [0] & [I] \end{bmatrix}.$$

Substitution of equation (32) into equation (9) and pre-multiplication by $[\bar{\Phi}]^{\mathrm{T}}$ yields

$$[\bar{M}]\{\ddot{q}\} + [\bar{C}]\{\dot{q}\} + [\bar{K}]\{q\} = \{\bar{Q}\}, \tag{33}$$

where the terms in equation (33) are

$$[\bar{M}] = \begin{bmatrix} M_{\theta\theta} & \{M_{\theta f}\}[\phi] \\ sym. & [\phi]^{\mathrm{T}}[M_{ff}][\phi] \end{bmatrix}, \tag{34}$$

$$[\bar{K}] = \begin{bmatrix} 1 & \{0\} \\ \{0\} & [\phi]^{\mathrm{T}}[K_{ff}][\phi] \end{bmatrix} = \begin{bmatrix} 0 & \{0\} & \{0\} \\ \{0\} & [\omega^2] & \{0\} \\ \{0\} & [0] & [K_{ff}^{ir}]^{\mathrm{T}}[Y] + [K_{ff}^{rr}] \end{bmatrix}, \tag{35}$$

$$[\bar{C}] = \begin{bmatrix} 0 & \{0\} \\ \{0\} & [\phi]^{\mathrm{T}}[C_{ff}][\phi] \end{bmatrix}, \tag{36}$$

$$[\bar{Q}] = [\bar{\Phi}]^{\mathrm{T}}\{\{Q_e\} + \{Q_v\}\}, \qquad \{q\} = \begin{Bmatrix} \theta \\ \{\eta\} \end{Bmatrix} = \begin{Bmatrix} \theta \\ \{\alpha\} \\ \{e_f^r\} \end{Bmatrix}. \tag{37, 38}$$

The mass, damping, and stiffness matrices of the flexible body, as well as the load vector are assembled first based on the three-dimensional solid element formulation of section 2.3. Subsequently, the matrices $[T]$, $[H]$, $[T_2]$, and $[T_3]$ are calculated using a Gaussian numerical integration scheme (equations (B.1)–(B.4)), and the matrices and load vectors of equation (9) are computed. Finally, the reduced equations (33) are formed after the modal transformation matrix $[\bar{\Phi}]$ is computed and are solved for the coupled rigid–flexible system response.

## 3. NUMERICAL SOLUTION

In this section the numerical algorithms employed for solving the equations of motion are presented. The Newmark method, modified by a Newton–Raphson iterative process within

each time step, is employed for the time integration. The incorporation of an iterative algorithm within each time step is necessary because the equations of motion contain non-linear terms in the mass matrix and the forcing vectors. Two specialized numerical solutions are developed in order to account for the representation of the flexible d.o.f. either as physical d.o.f. of a finite formulation or as retained and internal d.o.f. of a Craig–Bampton formulation. The Newmark method is used for the time integration of the governing equations. Due to the non-linear terms in the governing equations, an iterative algorithm based on the Newton–Raphson method is used at each time step during the time integration. The derivatives of the non-linear terms in the governing equations (9) with respect to the primary variables $\theta$ and $\{e_f\}$ are required by the Newton–Raphson iterative solution process. The vector $\{e_f\}$ represents the flexural d.o.f. Depending on the representation of the flexural d.o.f. either as d.o.f. of a finite element formulation or as retained and internal d.o.f. of a Craig–Bampton formulation, the numerical solution is developed approximately.

### 3.1. NUMERICAL SOLUTION BASED ON THE PHYSICAL D.O.F. OF A FINITE ELEMENT FORMULATION

The derivatives of the non-linear terms are calculated for each finite element and presented in the form of the $[PF^e]$, $[B^e]$, and $[P^e]$ matrices. The superscript "$e$" indicates an element matrix. Subsequently, the element matrices are assembled to form the corresponding global matrices $[PF]$, $[B]$, and $[P]$ (see equation (44)).

The element matrix $[PF^e]$ is defined as

$$[PF^e] = \begin{bmatrix} 0 & 2\{e\}^{\mathrm{T}}[T^e]\ddot{\theta} - \{\ddot{e}_f\}^{\mathrm{T}}[H^e] \\ \{0\} & -[H^e]\ddot{\theta} \end{bmatrix} \tag{39}$$

and originates from the differentiation of the non-linear term associated with the mass matrix, with respect to the rigid and flexible d.o.f. The element matrix $[B^e]$ is defined as

$$[B^e] = \begin{bmatrix} 0 & \{F\}^{\mathrm{T}}[A]^{\mathrm{T}}[A_\theta][N] - 2\{\dot{e}_f\}^{\mathrm{T}}[T^e]\dot{\theta} \\ \{0\} & [T^e]\dot{\theta}^2 - [T_2^e] - [T_3^e] \end{bmatrix} \tag{40}$$

and is derived by differentiating the forcing vector $\{Q_v\} + \{Q_e\}$ with respect to $\theta$ and $\{e_f\}$. Finally, the element matrix $[P^e]$ is defined as

$$[P^e] = \begin{bmatrix} -2\{e\}^{\mathrm{T}}[T^e]\{\dot{e}_f\} & -2\{e\}^{\mathrm{T}}[T^e]\dot{\theta} \\ 2[T^e]\{e\}\dot{\theta} + 2[H^e]\{\dot{e}_f\} - [[T_{2\dot{\theta}}^e] + [T_{3\dot{\theta}}^e]]\{e_f\} & 2[H^e]\dot{\theta} \end{bmatrix} \tag{41}$$

and originates from the differentiation of the forcing vector $\{Q_v\} + \{Q_e\}$ with respect to $\dot{\theta}$ and $\{\dot{e}_f\}$. The element matrices $[T_{2\dot{\theta}}^e]$ and $[T_{3\dot{\theta}}^e]$ in equation (41) are defined as

$$[T_{2\dot{\theta}}^e] = \frac{\partial[T_2^e]}{\partial\dot{\theta}} \quad \text{and} \quad [T_{3\dot{\theta}}^e] = \frac{\partial[T_3^e]}{\partial\dot{\theta}}. \tag{42}$$

The system of equations to be solved at the "$n+1$" time step of the Newmark time integration can be expressed as

$$[AK]_{n+1}^i \{\Delta q\}_{n+1}^{i+1} = \{R\}_{n+1}^i. \tag{43}$$

The superscript "$i$" indicates the $i$th Newton–Raphson iteration for the "$n+1$" time step. In equation (43), the system matrix $[AK]^i_{n+1}$ and the forcing vector $\{R\}^i_{n+1}$ are calculated at the $i$th iteration of the $(n+1)$th time step. The vector $\{\Delta q\}^{i+1}_{n+1}$ represents the change in the vector of variables $\{q_f\} = \{^{\theta}_{\{e_f\}}\}$ at the $(i+1)$th iteration of the $(n+1)$th time step. The matrix $[AK]^i_{n+1}$ and the vector $\{R\}^i_{n+1}$ in equation (43) are defined as

$$[AK]^i_{n+1} = a_2[M]^i_{n+1} + a_1[C] + [K] + [PF]^i_{n+1} - a_1[P]^i_{n+1} - [B]^i_{n+1}, \tag{44}$$

$$\{R\}^i_{n+1} = \{Q_e\}^i_{n+1} + \{Q_v\}^i_{n+1} + [M]^i_{n+1}\{R_1\} - [P]^i_{n+1}\{R_2\} + [C]\{R_3\} - [K]\{q_f\}^i_{n+1}, \tag{45}$$

where $a_1$ and $a_2$ are constants determined by the Newmark parameters and the selected time step. Superscript "$i$" indicates the $i$th Newton–Raphson iteration and subscript $(n+1)$ indicates the $(n+1)$th time step. Matrices $[M]$, $[C]$, and $[K]$ correspond to the mass, damping, and stiffness matrices of equation (9). $\{Q_v\}$ and $\{Q_e\}$ are the global arrays that correspond to the element vectors defined in equations (10) and (14) respectively. $[PF]$, $[B]$, and $[P]$ are the global matrices that originate from equations (39), (40), and (41) respectively. Vectors $\{R_1\}$, $\{R_2\}$, and $\{R_3\}$ contain information about the converged solution of the previous time step according to the standard Newmark time integration process.

The solution of equation (43) provides the change of the primary variables within each iteration of the $(n+1)$th time step. The Newton–Raphson iterative process is repeated until convergence is achieved. Then the solution process advances to the following time step and a new set of Newton–Raphson iterations is preformed. Since the body system is different at sequential time steps the converged solution at the $n$th time step is transformed from the body system of time step $n$ to the body system of time step $(n+1)$ during the solution process.

### 3.2. NUMERICAL SOLUTION BASED ON THE CMS FORMULATION

Since the flexible d.o.f. are different in the CMS-based formulation from the formulation presented in section 3.1, the differentiation of the non-linear terms in the equation of motions occurs with respect to a different set of primary variables. Thus, a separate formulation is required for the final system of equations within each iteration of every time step. The derivatives of the non-linear terms with respect to the CMS-based d.o.f. are presented in terms of the global matrices $[PF]$, $[B]$, and $[P]$.

The matrix $[PF]$ originates from the differentiation of the non-linear terms associated with the mass matrix $[\bar{M}]$ (equation (34)) with respect to $\theta$ and $\{\eta\}$ and is defined as

$$[PF] = \begin{bmatrix} 0 & 2(\{e_0\}^{\mathrm{T}} + \{\eta\}^{\mathrm{T}}[\phi]^{\mathrm{T}})[T][\phi]\ddot{\theta} - \{\ddot{\eta}\}^{\mathrm{T}}[\phi]^{\mathrm{T}}[H][\phi] \\ \{0\} & -[\phi]^{\mathrm{T}}[H][\phi]\ddot{\theta} \end{bmatrix},$$

where

$$[\phi] = \begin{bmatrix} [X] & [Y] \\ [0] & [I] \end{bmatrix} \tag{46}$$

is the CMS modal matrix.

The matrix $[B]$ originates from the differentiation of the forcing vector $\{\bar{Q}\}$ with respect to $\theta$ and $\{\eta\}$ and is defined as

$$[B] = \begin{bmatrix} 0 & \{b\}^{\mathrm{T}}[\phi] - 2\dot{\theta}\{\dot{\eta}\}^{\mathrm{T}}[\phi]^{\mathrm{T}}[T][\phi] \\ \{0\} & [\phi]^{\mathrm{T}}[[T]\dot{\theta}^2 - [T_2] - [T_3]][\phi] \end{bmatrix}, \tag{47}$$

where the vector $\{b\}$ is defined as

$$\{b\} = \mathop{\mathrm{A}}_{e=1}^{NM} ([N]^{\mathrm{T}}[A_\theta]^{\mathrm{T}}[A]\{F\}). \tag{48}$$

The notation $\mathrm{A}_{e=1}^{NM}$ indicates assembling of element values over all the finite elements. Finally, matrix $[P]$ originates from the differentiation of the forcing vector $\{\bar{Q}\}$ with respect to $\dot{\theta}$ and $\{\dot{\eta}\}$ and is defined as

$$[P] = \begin{bmatrix} -2(\{e_0\}^{\mathrm{T}} + \{\eta\}^{\mathrm{T}}[\phi]^{\mathrm{T}})[T][\phi]\{\dot{\eta}\} & -2\dot{\theta}(\{e_0\}^{\mathrm{T}} + \{\eta\}^{\mathrm{T}}[\phi]^{\mathrm{T}})[T][\phi] \\ 2[\phi]^{\mathrm{T}}\{[T](\{e_0\} + [\phi]\{\eta\})\dot{\theta} - \tfrac{1}{2}[T_{23\dot{\theta}}][\phi]\{\eta\} + [H][\phi]\{\dot{\eta}\} & 2[\phi]^{\mathrm{T}}[H][\phi]\dot{\theta} \end{bmatrix}. \tag{49}$$

Matrix $[T_{23\dot{\theta}}]$ is defined as

$$[T_{23\dot{\theta}}] = \frac{\partial}{\partial\dot{\theta}}[[T_2] + [T_3]]. \tag{50}$$

The format of the system of linear equations to be solved at the $(i+1)$th Newton–Raphson iteration of the $(n+1)$th time step is identical with equation (43). Therefore, the format of the terms presented in equations (44) and (45) can be readily employed. Differences appear in the definition of the primary variables of the system of equations as $\{q\} = \{{}^{\theta}_{\{\eta\}}\}$ and the expressions of the matrices $[PF]$, $[B]$, and $[P]$ (equations (46), (47), and (49)). In the Craig–Bampton-based approach, the primary variable $\{q\} = \{{}^{\theta}_{\{\eta\}}\}$ contains the modal d.o.f. for the flexible motion. Thus, a specialized transformation is established between the modal d.o.f. of sequential time steps while the rest of the solution process remains the same with the one presented in section 3.1.

## 4. VALIDATION

Two rotating beam configurations are analyzed with the axis of rotation defined to be either vertical or along the longitudinal axis of the beam. For the former configuration an analytical solution, derived by the Galerkin method, is available and it is compared with the numerical results. For both configurations computations are performed by all the new finite element formulations. In order to validate the new developments, the numerical results are inspected for correlation to the analytical solution, and for convergence between the different formulations.

### 4.1. A BEAM ROTATING AROUND ITS VERTICAL AXIS

A rotating cantilever beam with a harmonic force excitation applied at the free tip is analyzed. This example is selected because an analytical solution that includes the rotation

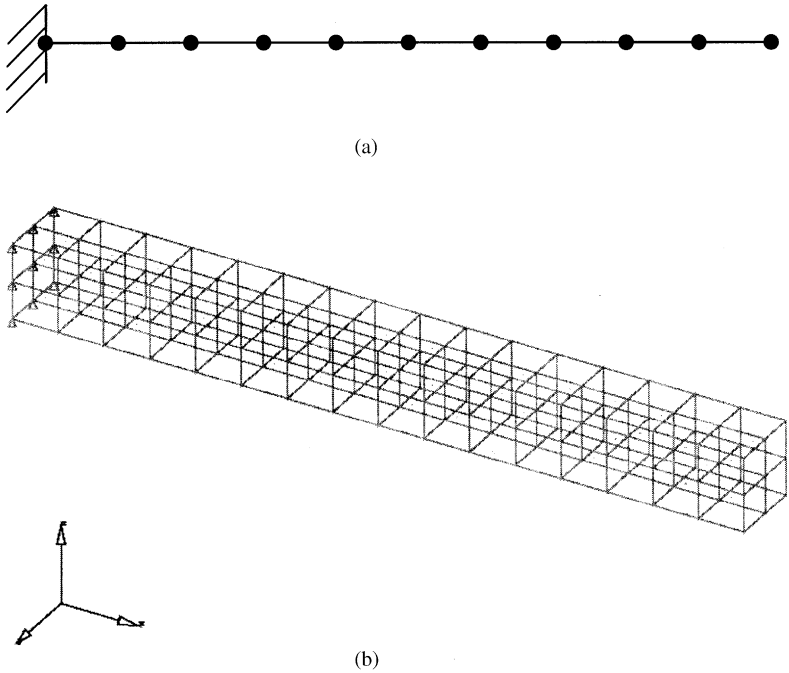

(a)

(b)

Figure 5. (a) 3D beam finite element model; (b) 3D solid finite element model.

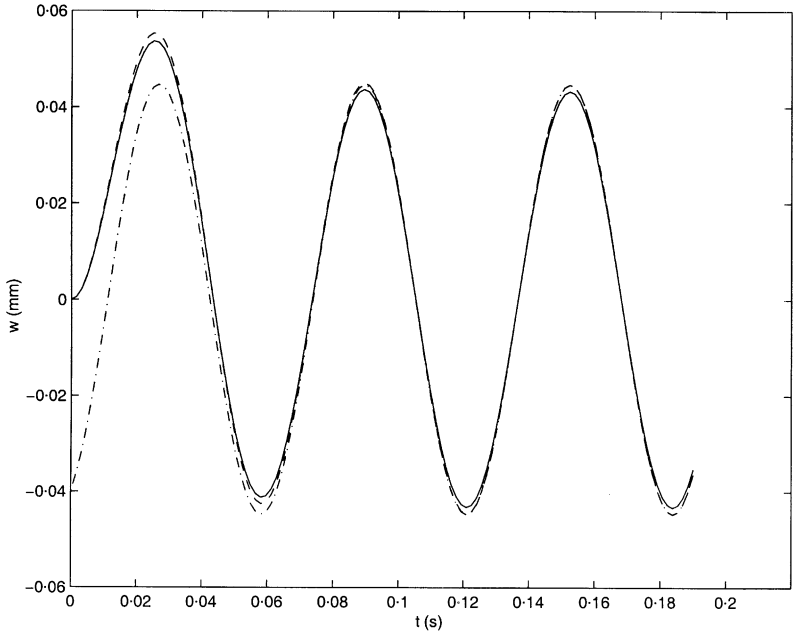


Figure 6. Vertical displacement ($z$-component) at the tip of the rotating beam for $\omega = 100$ rad/s and 1000 r.p.m.: −·−·−, analytical; - - - - -, beam FEA; ——, solid FEA; ·····, CMS d.o.f.

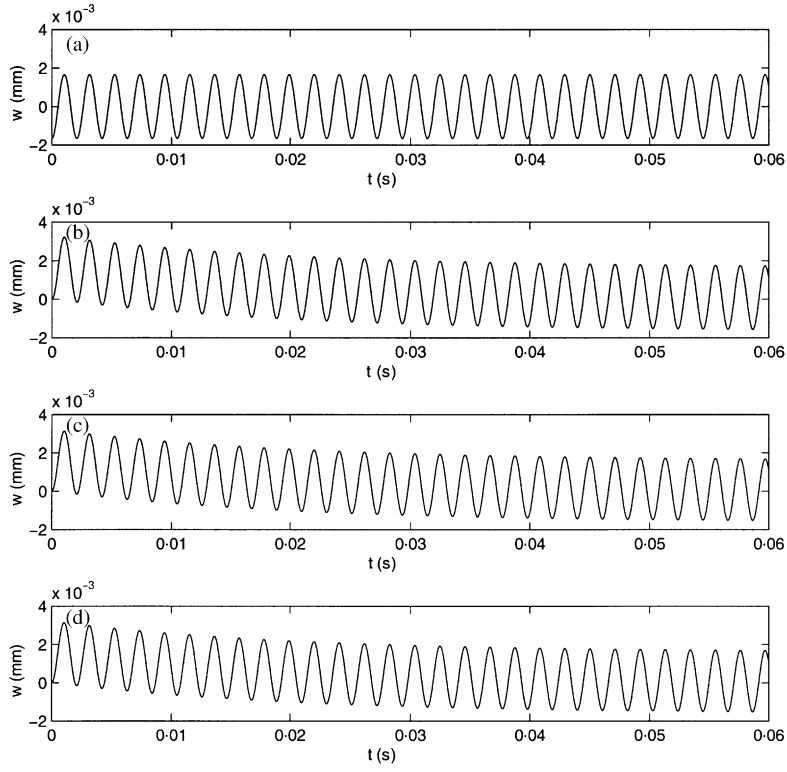


Figure 7. Vertical displacement ($z$-component) at the tip of the rotating beam for $\omega = 3000$ rad/s and 1000 r.p.m.: (a) analytical; (b) beam FEA; (c) solid FEA; (d) CMS d.o.f.

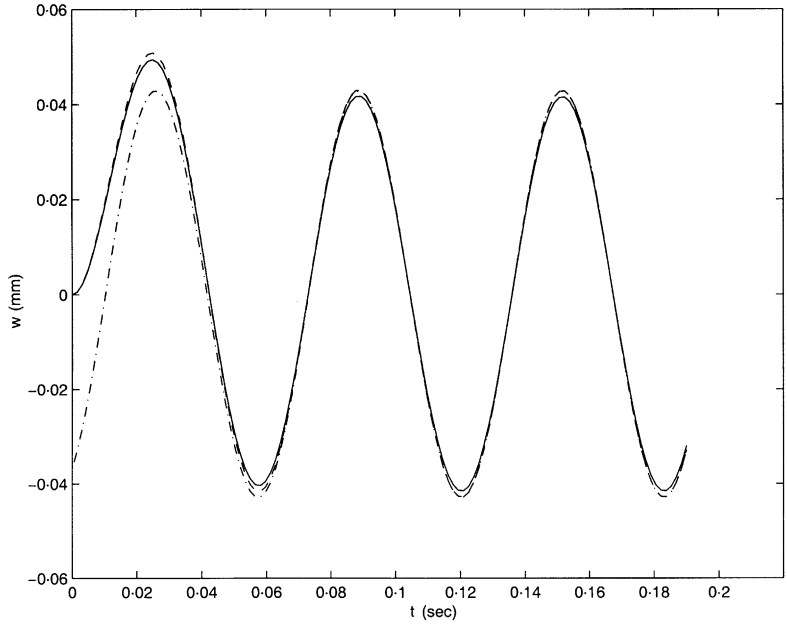


Figure 8. Vertical displacement ($z$-component) at the tip of the rotating beam for $\omega = 100$ rad/s and 10 000 r.p.m.: –·–·–, analytical; - - - - -, beam FEA; ——, solid FEA; ·····, CMS d.o.f.

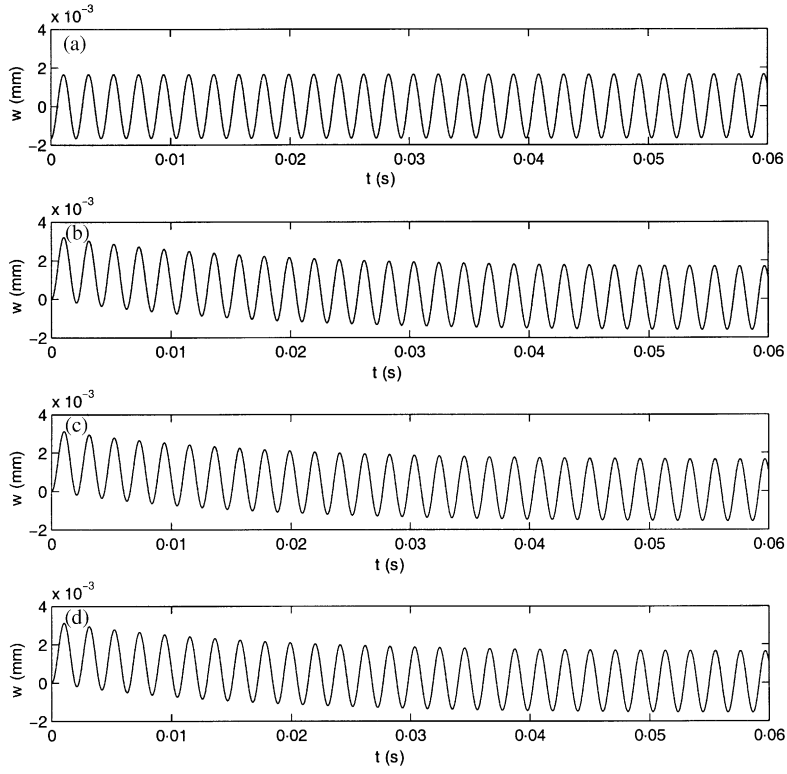


Figure 9. Vertical displacement ($z$-component) at the tip of the rotating beam for $\omega = 3000$ rad/s and 10 000 r.p.m.: (a) analytical; (b) beam FEA; (c) solid FEA; (d) CMS d.o.f.

effect and the non-linear correction from the work done by the centrifugal forces can be developed for the flexible response of the beam [15]. Analyses are performed in order to validate all three new formulations. Thus, the flexible behavior of the beam structure is modelled either with beam finite elements in a three-dimensional space or with solid finite elements or by the CMS internal and retained d.o.f. derived from a solid FEA model. Good correlation is observed among all three sets of numerical results and also between all the numerical results and the analytical solution. The beam configuration is presented in Figure 4. The dimensions are $200 \times 20 \times 20\,\text{mm}^3$ and the material properties are $E = 200\,\text{GPa}$ and $\rho = 7800\,\text{kg/m}^3$. Structural damping equal to 2% is specified. The sinusoidal force has magnitude equal to 100 N and direction parallel to the direction of the rigid-body rotation. Four combinations of two excitation frequencies for the harmonic force ($\omega_1 = 100$ rad/s and $\omega_2 = 3000$ rad/s) with two rotational speeds of $\Omega_1 = 1000$ r.p.m. and $\Omega_2 = 10\,000$ r.p.m. are employed in the analysis. The two excitation frequencies are selected based on the first three lowest natural frequencies of this beam ($\omega_{n1} = 2570$ rad/s, $\omega_{n2} = 16\,105$ rad/s, and $\omega_{n3} = 88\,365$ rad/s). The first excitation frequency is away from any resonant frequency and the second is in the vicinity of the first resonant frequency. Thus the validation is performed for off-resonance and close to resonance conditions. The second rotational speed is selected as 10 times the lower rotational speed in order to amplify the stiffening effects due to the rigid-body rotation and validate the expected trends in the numerical results.

The rotating cantilever beam is analyzed by all three new numerical formulations. The finite element models employed in the analyses are depicted in Figure 5. Ten finite elements

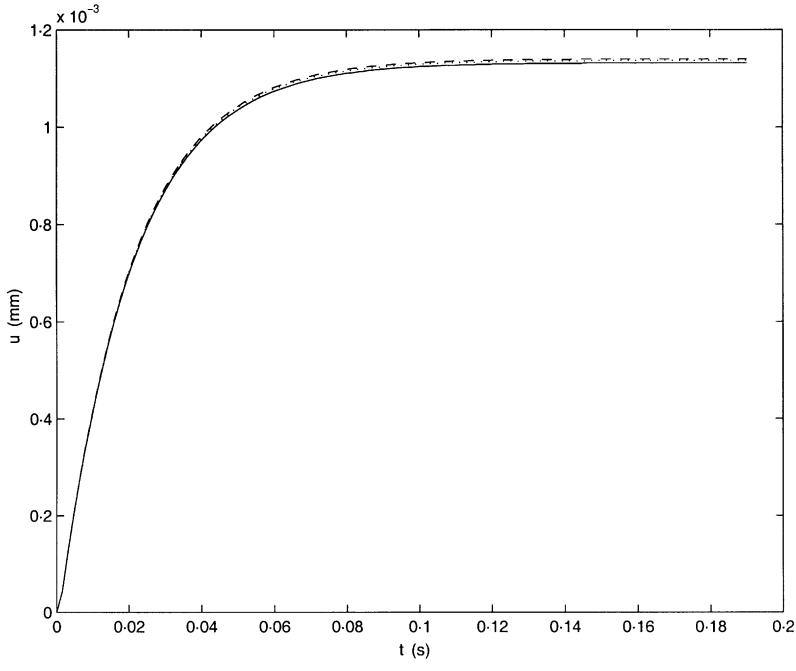


Figure 10. Axial displacement ($x$-component) at the tip of the rotating beam for $\omega = 100$ rad/s and 1000 r.p.m.: - - - - -, beam FEA; ——, solid FEA; ·····, CMS d.o.f.

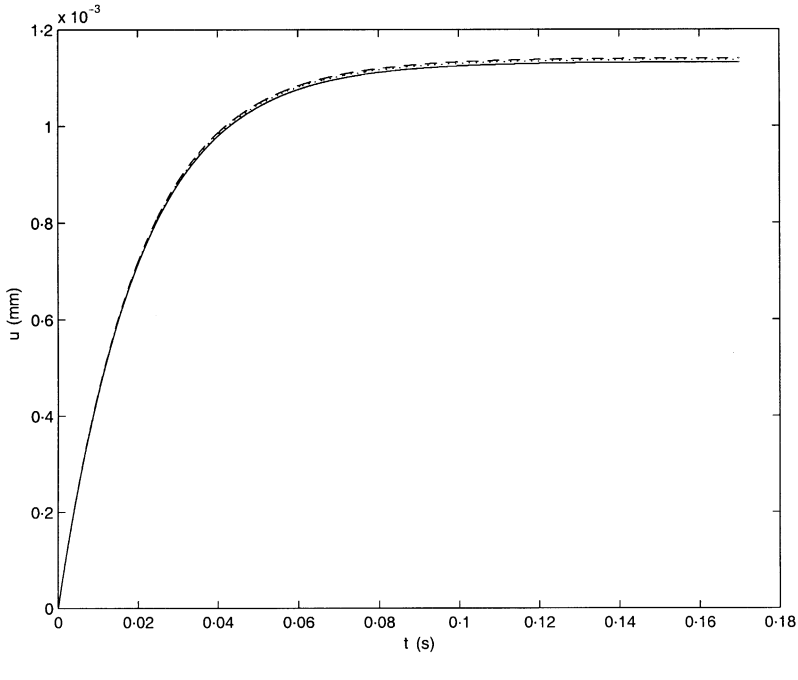


Figure 11. Axial displacement ($x$-component) at the tip of the rotating beam for $\omega = 3000$ rad/s and 1000 r.p.m.: - - - - -, beam FEA; ——, solid FEA; ·····, CMS d.o.f.

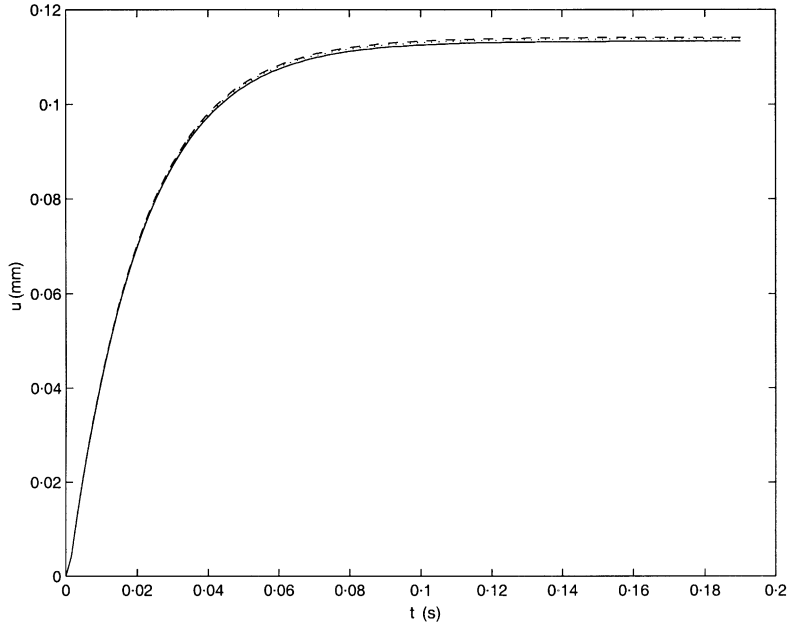


Figure 12. Axial displacement ($x$-component) at the tip of the rotating beam for $\omega = 100$ rad/s and 10 000 r.p.m.: - - - - -, beam FEA; ——, solid FEA; ·····, CMS d.o.f.

are employed in the beam model and 64 finite elements are employed in the solid model. The beam finite elements ensure continuity of both displacement and slope at the interfaces between elements while the solid elements ensure only continuity of displacement. Therefore, a larger number of solid finite elements than beam finite elements is used in the longitudinal direction in order to capture accurately the flexural deformation of the beam. All frequencies of analysis are well below the second natural frequency of the beam; therefore, the number of elements in both models are sufficient for capturing the expected deformation of the beam, and the two finite element based solutions are expected to produce similar results. Differences are expected in the results between the different methods anytime that the number of elements utilized in the finite element model is not enough to capture the flexible deformation of the beam.

The boundary conditions at the clamped end of the structure are imposed in the two finite element models by constraining the displacements and rotations of the fixed edge node in the beam model or by constraining all the displacements at the nodes on the fixed edge in the solid model. The CMS d.o.f. are computed from the solid model. All d.o.f. for the nodes on both the fixed edge and the mid-span cross-section are selected as retained d.o.f. The remaining d.o.f. constitute the internal d.o.f. Eight constraint modes are computed in the CMS formulation for this solid model.

Results for the vertical deflection ($z$-displacement) at the tip of the beam are presented in Figures 6–9 for the four operating conditions. In each figure, results from the analytical solution and the three numerical simulations are presented. Good correlation between all the numerical results and the analytical solution is observed once the initial transient effects are dissipated and the final steady state condition is reached. The convergence demonstrated by all three numerical solutions and their close agreement to the analytical solution validates the new theoretical developments and their implementation.

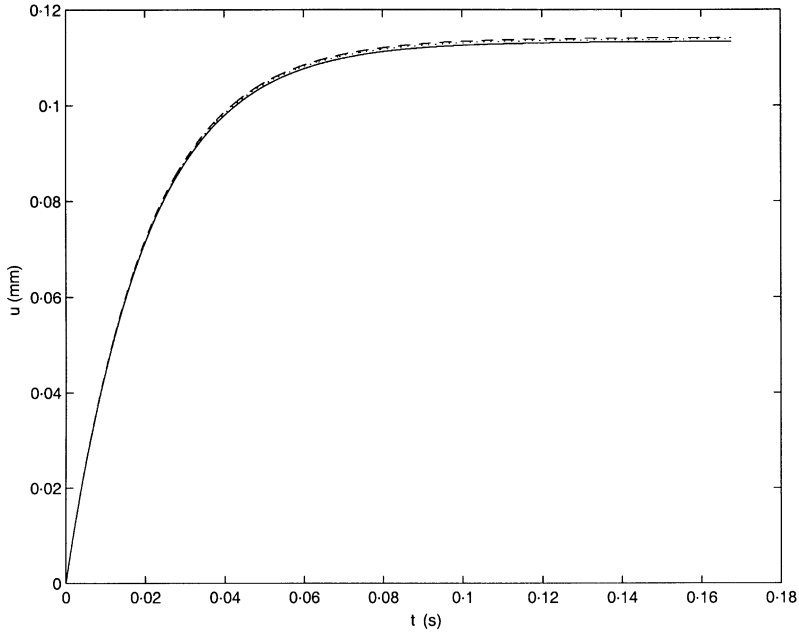


Figure 13. Axial displacement ($x$-component) at the tip of the rotating beam for $\omega = 3000$ rad/s and 10 000 r.p.m.: - - - - -, beam FEA; ——, solid FEA; ·····, CMS d.o.f.

By comparing the results corresponding to rotational speeds at 1000 and 10 000 r.p.m. (Figures 6 and 8 respectively) for the same excitation frequency ($\omega = 100$ rad/s), a slightly smaller tip displacement is demonstrated for the higher rotational speed. This is expected due to the non-linear stiffening effect generated from the rigid-body rotation.

The centrifugal force induces an axial deformation in the $x$ direction. The $x$-displacement at the tip of the rotating beam can be evaluated as

$$\Delta x = \int_0^L \frac{P_x}{aE}\,\mathrm{d}x = \frac{\rho\Omega^2 L^3}{3E}. \tag{51}$$

Therefore, the axial tip displacement for 1000 r.p.m. is $1{\cdot}14 \times 10^{-3}$ mm and for 10 000 r.p.m. is 0·114 mm. The axial tip displacements are presented in Figures 10–13 for the four operating conditions respectively. Good correlation is observed at the steady state between the expected tip displacement and the computational results from all three formulations.

### 4.2. A BEAM ROTATING AROUND ITS LONGITUDINAL AXIS

A simply supported beam rotating around its longitudinal axis ($x$-axis) (Figure 14) is also analyzed. The transformation matrix $[A]$ (equation (16)) must reflect the geometry of the configuration that is analyzed. Therefore, equations (16)–(18) are modified based on the change introduced in the transformation matrix resulting in

$$[A] = \begin{bmatrix} 1 & 0 & 0 \\ 0 & \cos\theta & -\sin\theta \\ 0 & \sin\theta & \cos\theta \end{bmatrix}, \qquad [A_\theta] = \frac{\mathrm{d}[A]}{\mathrm{d}\theta} = \begin{bmatrix} 0 & 0 & 0 \\ 0 & -\sin\theta & -\cos\theta \\ 0 & \cos\theta & -\sin\theta \end{bmatrix}, \tag{52, 53}$$

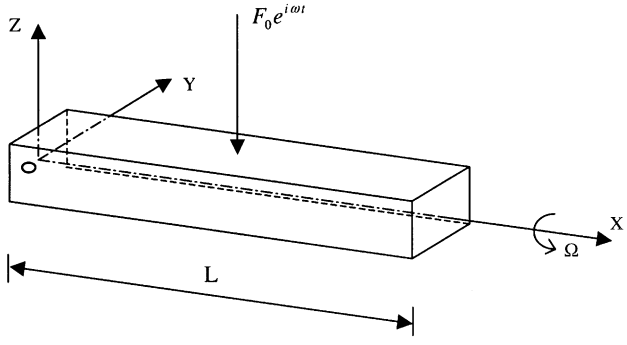


Figure 14. A beam rotating around its longitudinal axis ($X$-axis).

$$[A_{\theta\theta}] = \frac{\mathrm{d}[A_\theta]}{\mathrm{d}\theta} = \begin{bmatrix} 0 & 0 & 0 \\ 0 & -\cos\theta & \sin\theta \\ 0 & -\sin\theta & -\cos\theta \end{bmatrix}, \tag{54}$$

$$[A_\theta]^{\mathrm{T}}[A_\theta] = \begin{bmatrix} 0 & 0 & 0 \\ 0 & 1 & 0 \\ 0 & 0 & 1 \end{bmatrix}, \quad [A_\theta]^{\mathrm{T}}[A] = \begin{bmatrix} 0 & 0 & 0 \\ 0 & 0 & 1 \\ 0 & -1 & 0 \end{bmatrix}. \tag{55}$$

The change introduced in the transformation matrix and its derivative matrix propagates to the element matrices $[T^e]$ and $[H^e]$, which are defined in equation (8). Finally, by considering a concentrated force applied vertically at the mid-span of the beam ($z$ direction in the global co-ordinate system), the generalized external forcing vector becomes

$$\{Q_e\} = \begin{Bmatrix} \{e\}^{\mathrm{T}}[N]^{\mathrm{T}}[A_\theta]^T\{F\} \\ [N]^{\mathrm{T}}[A]^{\mathrm{T}}\{F\} + [T]\{e_f\}\dot{\theta}^2 \end{Bmatrix}. \tag{56}$$

The force vector $\{F\}$ is expressed in the global co-ordinate system and the term $[T]\{e_f\}\dot{\theta}^2$ is derived from the virtual work done by the centrifugal force due to the flexible motion. The latter term represents the influence of the centrifugal force on the flexible displacements along the lateral and the vertical directions.

The element matrices $[B^e]$ (equation (40)) and $[P^e]$ (equation (41)) are derived through differentiation of the forcing vector. Thus the information provided by equation (56) is employed in the definition of the element matrices $[B^e]$ and $[P^e]$ for the solid finite element formulation:

$$[B^e] = \begin{bmatrix} \{e\}^{\mathrm{T}}[N]^{\mathrm{T}}\{A_{\theta\theta}\}^{\mathrm{T}}\{F\} & \{F\}^{\mathrm{T}}[A_\theta][N] - 2\{\dot{e}_f\}^{\mathrm{T}}[T^e]\dot{\theta} \\ [N]^{\mathrm{T}}[A_\theta]^{\mathrm{T}}\{F\} & 2[T^e]\dot{\theta}^2 \end{bmatrix}, \tag{57}$$

$$[P^e] = \begin{bmatrix} -2\{e\}^{\mathrm{T}}[T^e]\{\dot{e}_f\} & -2\{e\}^{\mathrm{T}}[T^e]\dot{\theta} \\ 2[T^e]\{e\}\dot{\theta} + 2[T]\{e_f\}\dot{\theta} + 2[H^e]\{\dot{e}_f\} & 2[H^e]\dot{\theta} \end{bmatrix}. \tag{58}$$

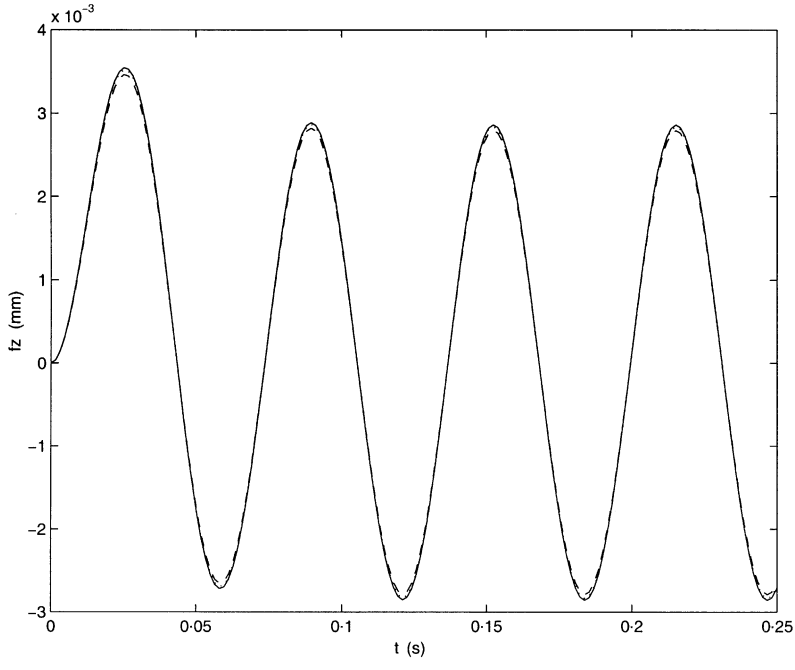


Figure 15. Vertical displacement ($z$-component) at the mid-span of the rotating simply supported beam for $\omega = 100$ rad/s and 100 r.p.m.: -------, beam FEA; ——, solid FEA; ·····, CMS d.o.f.

Similarly, the definition of matrices $[B]$ and $[P]$ in the CMS formulation (equations (47) and (49)) is modified in order to reflect the present form of the forcing vector $\{Q_e\}$:

$$[B] = \begin{bmatrix} (\{e_0\}^{\mathrm{T}} + \{\eta\}^{\mathrm{T}}[\phi]^{\mathrm{T}})\{bb\} & \{b\}^{\mathrm{T}}[\phi] - 2\dot{\theta}\{\dot{\eta}\}^{\mathrm{T}}[\phi]^{\mathrm{T}}[T][\phi] \\ [\phi]^{\mathrm{T}}\{b\} & 2[\phi]^{\mathrm{T}}[T][\phi]\dot{\theta}^2 \end{bmatrix}, \tag{59}$$

$$[P] = \begin{bmatrix} -2(\{e_0\}^{\mathrm{T}} + \{\eta\}^{\mathrm{T}}[\phi]^{\mathrm{T}})[T][\phi]\{\dot{\eta}\} & -2\dot{\theta}(\{e_0\}^{\mathrm{T}} + \{\eta\}^{\mathrm{T}}[\phi]^{\mathrm{T}})[T][\phi] \\ 2[\phi]^{\mathrm{T}}\{[T](\{e_0\} + [\phi]\{\eta\})\dot{\theta} + [H][\phi]\{\dot{\eta}\}\} & 2[\phi]^{\mathrm{T}}[H][\phi]\dot{\theta} \end{bmatrix}, \tag{60}$$

where currently vectors $\{b\}$ and $\{bb\}$ are defined as

$$\{b\} = \sum_{e=1}^{NM} ([N]^{\mathrm{T}}[A_\theta]^{\mathrm{T}}[F]), \qquad [bb\} = \sum_{e=1}^{NM} ([N]^{\mathrm{T}}[A_{\theta\theta}]^{\mathrm{T}}[F]). \tag{61, 62}$$

Analysis are performed for three rotational speeds: 100, 1000, and 5000 r.p.m. The frequency of the external force is retained constant at $\omega = 100$ rad/s for all three rotational speeds. Analyses are performed by all three new formulations. Results for the vertical displacements along the direction of the load ($Z$ direction) at the location where the load is applied is presented in Figures 15–17 for all three r.p.m. In each case the results from all three solutions are almost identical. For the analyzed configuration the differences in the rotational speed have a minimal effect in the $Z$ direction. The lateral displacements in the direction perpendicular to the external load at the location of the load are three orders of

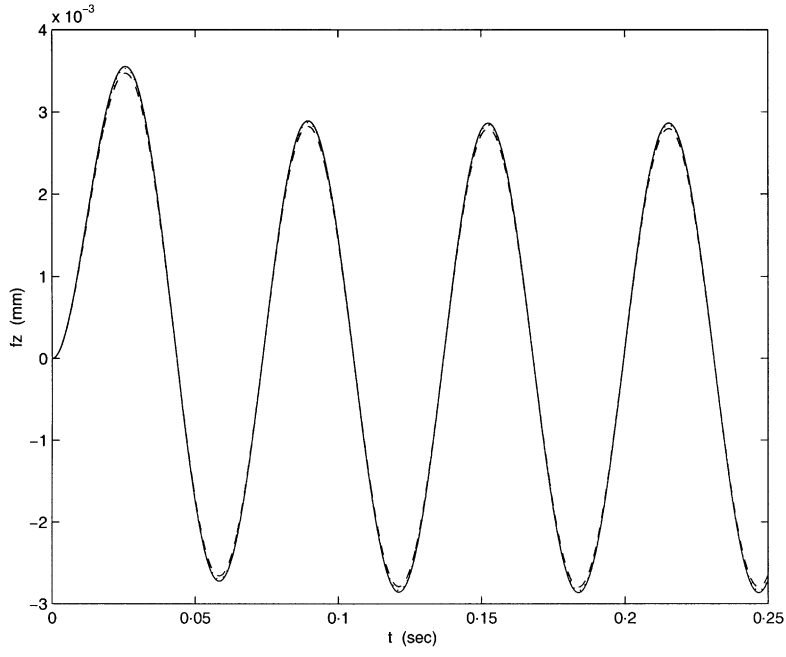


Figure 16. Vertical displacement ($z$-component) at the mid-span of the rotating simply supported beam for $\omega = 100$ rad/s and 1000 r.p.m.: - - - - - - -, beam FEA; ——, solid FEA; ·····, CMS d.o.f.

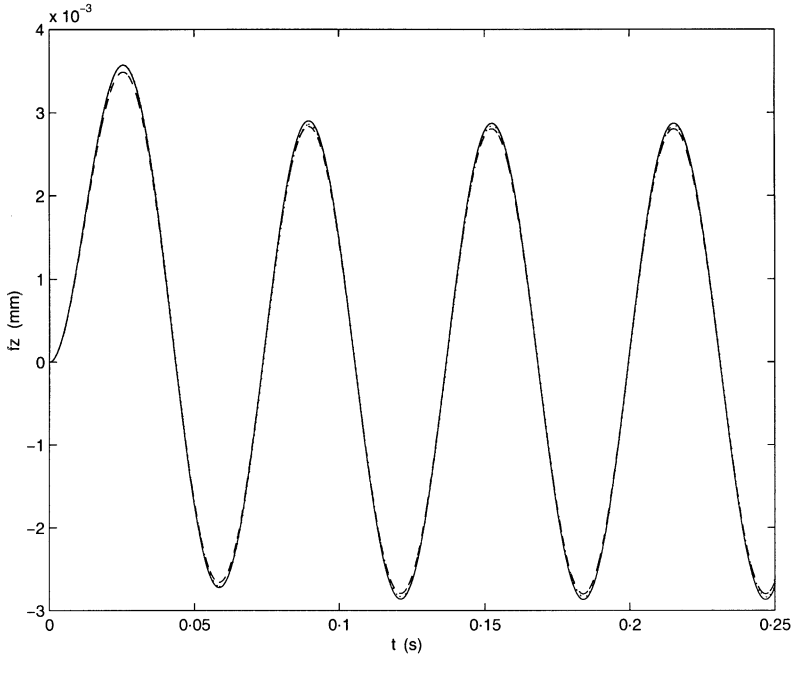


Figure 17. Vertical displacement ($z$-component) at the mid-span of the rotating simply supported beam for $\omega = 100$ rad/s and 5000 r.p.m.: - - - - - - -, beam FEA; ——, solid FEA; ·····, CMS d.o.f.

magnitude smaller than the displacements in the $Z$ direction. This observation is consistent with the minimal effect exhibited by the rotational speed in the analyzed configuration.

## 5. CONCLUSIONS

Based on an existing comprehensive formulation for rotating flexible systems, a new finite element based formulation for coupling the rigid- and flexible-body dynamics for rotating beams was presented in this paper. The flexible d.o.f. were represented either as finite element d.o.f. of beam finite elements in a three-dimensional space or as finite element d.o.f. of three-dimensional solid elements or finally as internal and retained d.o.f. of a Craig–Bampton formulation. The coupling matrices between the rigid-body rotation and the flexible d.o.f. were developed accordingly. The non-linear effects from the work done by the centrifugal forces were also included. The coupled system of equations was solved in the time domain using the Newmark method while the Newton–Raphson method was employed for solving the non-linear system of equations within each time step. The three new formulations were validated using the analytical solution of a rotating cantilever beam under a harmonic force excitation at its free tip. The analytical solution included the rotation effect and the non-linear correction from the work done by the centrifugal forces on the flexible response of the beam. Very good correlation was observed between the numerical results from all three formulations and the analytical solution after the initial transient effects were dissipated and the final steady state condition was reached. The convergence demonstrated by all three formulations and their close agreement to the analytical solution validates the new theoretical developments and their implementation. A beam rotating around its longitudinal axis was also analyzed. The validity of the new developments was demonstrated by the consistently good agreement observed between the three different new formulations.

## ACKNOWLEDGMENTS

The completion of this work was made possible through support by NSF grant No. CMS-9713793.

## REFERENCES

1. T. R. Kane, R. R. Ryan and A. K. Banerjee 1987 *Journal of Guidance, Control, and Dynamics* **10**, 139–151. Dynamics of a cantilever beam attached to a moving base.
2. A. Yigit, R. A. Scott and A. Galip Ulsoy 1988 *Journal of Sound and Vibration* **121**, 201–210. Flexural motion of a radially rotating beam attached to a rigid body.
3. J. D. Downer, K. C. Park and J. C. Chiou 1992 *Computer Methods in Applied Mechanics and Engineering* **96**, 373–408. Dynamics of flexible beams for multibody systems: a computational procedure.
4. J. W.-Z. Zu and R. P. S. Han 1992 *Journal of Applied Mechanics* **59**, 197–204. Natural frequencies and normal modes of a spinning Timoshenko beam with general boundary conditions.
5. W. J. Hearing, R. R. Ryan and R. A. Scott 1994 *Journal of Guidance, Control, and Dynamics* **17**, 76–83. New formulation for flexible beams undergoing large overall plane motion.
6. M. Iura and S. N. Atluri 1995 *Computers and Structures* **55**, 453–462. Dynamic analysis of planar flexible beams with finite rotations by using inertial and rotating frames.
7. A. Ibrahimbegovic and S. Mamouri 1999 *Computers and Structures* **70**, 1–22. Nonlinear dynamics of flexible beams in planar motion: formulation and time-stepping scheme for stiff problems.
8. D. J. Segalman and C. R. Dohrmann 1996 *Journal of Vibration and Acoustics* **118**, 313–317. A method for calculating the dynamics of rotating flexible structures. Part 1: derivation.

9. M. D. AL-ANSARY 1998 *Computers and Structures* **69**, 321–328. Flexural vibrations of rotating beams considering rotary inertia.
10. W. PAN and E. J. HAUG 1999 *Computer Methods in Applied Mechanics and Engineering* **173**, 189–200. Flexible multibody dynamic simulation using optimal lumped inertia matrices.
11. J. MAYO, J. DOMINGUEZ and A. A. SHABANA 1995 *Journal of Vibration and Acoustics* **117**, 501–509. Geometrically nonlinear formulations of beams in flexible multibody dynamics.
12. H. EL-ABSY and A. A. SHABANA 1996 *Journal of Sound and Vibration* **198**, 617–637. Coupling between rigid body and deformation modes.
13. M. A. BROWN and A. A. SHABANA 1997 *Journal of Sound and Vibration* **204**, 439–457. Application of multibody methodology to rotating shaft problems.
14. R. R. CRAIG JR and M. C. C. BAMPTON 1968 *American Institute of Aeronautics and Astronautics Journal* **6**, 1313–1319. Coupling of substructures for dynamic analysis.
15. L. MEIROVITCH 1967 *Analytical Methods in Vibrations*. New York: Macmillan Publishing Co, Inc.
16. A. A. SHABANA 1998 *Dynamics of Multibody System*. Cambridge: Cambridge University Press; second edition.
17. J. S. PRZEMIENIECKI 1968 *Theory of Matrix Structural Analysis*. New York: McGraw-Hill.
18. S. S. RAO 1989 *The Finite Element Method in Engineering*. Oxford: Pergamon Press; second edition.
19. W. CHUANG 1991 *Ph.D. Dissertation, University of Michigan, Ann Arbor*. Analysis of the crankshaft/main-bearings system of a multi-cylinder engine.
20. R. R. CRAIG JR 1981 *Structural Dynamics*. New York: John Wiley & Sons.

## APPENDIX A: DEFINITION OF ELEMENT MATRICES FOR BEAM FINITE ELEMENTS IN A THREE-DIMENSIONAL SPACE

$$[T^e] = \rho a l \begin{bmatrix} \frac{1}{3} & 0 & 0 & 0 & 0 & 0 & \frac{1}{6} & 0 & 0 & 0 & 0 & 0 \\ & \frac{13}{35} & 0 & 0 & 0 & \frac{11}{210}l & 0 & \frac{9}{70} & 0 & 0 & 0 & -\frac{13}{420}l \\ & & 0 & 0 & 0 & 0 & 0 & 0 & 0 & 0 & 0 & 0 \\ & & & 0 & 0 & 0 & 0 & 0 & 0 & 0 & 0 & 0 \\ & & & & 0 & 0 & 0 & 0 & 0 & 0 & 0 & 0 \\ & & & & & \frac{1}{105}l^2 & 0 & \frac{13}{420}l & 0 & 0 & 0 & -\frac{1}{140}l^2 \\ & & & & & & \frac{1}{3} & 0 & 0 & 0 & 0 & 0 \\ & & & & & & & \frac{13}{35} & 0 & 0 & 0 & -\frac{11}{210}l \\ & & & & & & & & 0 & 0 & 0 & 0 \\ & & & & & & & & & 0 & 0 & 0 \\ & sym. & & & & & & & & & 0 & 0 \\ & & & & & & & & & & & \frac{1}{105}l^2 \end{bmatrix}_{12\times 12}, \tag{A.1}$$

$$[H^e] = \rho a l \begin{bmatrix} 0 & \frac{7}{20} & 0 & 0 & 0 & \frac{1}{20}l & 0 & \frac{3}{20} & 0 & 0 & 0 & -\frac{1}{30}l \\ -\frac{7}{20} & 0 & 0 & 0 & 0 & 0 & -\frac{3}{20} & 0 & 0 & 0 & 0 & 0 \\ 0 & 0 & 0 & 0 & 0 & 0 & 0 & 0 & 0 & 0 & 0 & 0 \\ 0 & 0 & 0 & 0 & 0 & 0 & 0 & 0 & 0 & 0 & 0 & 0 \\ 0 & 0 & 0 & 0 & 0 & 0 & 0 & 0 & 0 & 0 & 0 & 0 \\ -\frac{1}{20}l & 0 & 0 & 0 & 0 & 0 & -\frac{1}{30}l & 0 & 0 & 0 & 0 & 0 \\ 0 & \frac{3}{20} & 0 & 0 & 0 & \frac{1}{30}l & 0 & \frac{7}{20} & 0 & 0 & 0 & -\frac{1}{20}l \\ -\frac{3}{20} & 0 & 0 & 0 & 0 & 0 & -\frac{7}{20} & 0 & 0 & 0 & 0 & 0 \\ 0 & 0 & 0 & 0 & 0 & 0 & 0 & 0 & 0 & 0 & 0 & 0 \\ 0 & 0 & 0 & 0 & 0 & 0 & 0 & 0 & 0 & 0 & 0 & 0 \\ 0 & 0 & 0 & 0 & 0 & 0 & 0 & 0 & 0 & 0 & 0 & 0 \\ \frac{1}{30}l & 0 & 0 & 0 & 0 & 0 & \frac{1}{20}l & 0 & 0 & 0 & 0 & 0 \end{bmatrix}_{12\times 12}, \tag{A.2}$$

$$[T_2^e] = \frac{1}{2}\rho a\Omega^2 \begin{bmatrix}
0 & 0 & 0\ 0\ 0 & 0 & 0 & 0 & 0\ 0\ 0 & 0 \\
0 & -\frac{12l}{35} - \frac{6x_0}{5} + \frac{6}{5}\frac{L^2 - x_0^2}{l} & 0\ 0\ 0 & -\frac{l^2}{14} - \frac{x_0 l}{5} + \frac{L^2 - x_0^2}{10} & 0 & \frac{12l}{35} + \frac{6x_0}{5} - \frac{6}{5}\frac{L^2 - x_0^2}{l} & 0\ 0\ 0 & \frac{l^2}{35} + \frac{L^2 - x_0^2}{10} \\
0 & 0 & 0\ 0\ 0 & 0 & 0 & 0 & 0\ 0\ 0 & 0 \\
0 & 0 & 0\ 0\ 0 & 0 & 0 & 0 & 0\ 0\ 0 & 0 \\
0 & 0 & 0\ 0\ 0 & 0 & 0 & 0 & 0\ 0\ 0 & 0 \\
0 & -\frac{l^2}{14} - \frac{x_0 l}{5} + \frac{L^2 - x_0^2}{10} & 0\ 0\ 0 & -\frac{2l^3}{105} + \frac{2(L^2 - x_0^2)l - x_0 l^2}{15} & 0 & \frac{l^2}{14} + \frac{x_0 l}{5} - \frac{L^2 - x_0^2}{10} & 0\ 0\ 0 & \frac{l^3}{70} + \frac{x_0 l^2 - L^2 l + x_0^2 l}{30} \\
0 & 0 & 0\ 0\ 0 & 0 & 0 & 0 & 0\ 0\ 0 & 0 \\
0 & \frac{12l}{35} + \frac{6x_0}{5} - \frac{6}{5}\frac{L^2 - x_0^2}{l} & 0\ 0\ 0 & \frac{l^2}{14} + \frac{x_0 l}{5} - \frac{L^2 - x_0^2}{10} & 0 & -\frac{12l}{35} - \frac{6x_0}{5} + \frac{6}{5}\frac{L^2 - x_0^2}{l} & 0\ 0\ 0 & -\frac{l^2}{35} - \frac{L^2 - x_0^2}{10} \\
0 & 0 & 0\ 0\ 0 & 0 & 0 & 0 & 0\ 0\ 0 & 0 \\
0 & 0 & 0\ 0\ 0 & 0 & 0 & 0 & 0\ 0\ 0 & 0 \\
0 & 0 & 0\ 0\ 0 & 0 & 0 & 0 & 0\ 0\ 0 & 0 \\
0 & \frac{l^2}{35} + \frac{L^2 - x_0^2}{10} & 0\ 0\ 0 & \frac{l^3}{70} + \frac{x_0 l^2 - L^2 l + x_0^2 l}{30} & 0 & -\frac{l^2}{35} - \frac{L^2 - x_0^2}{10} & 0\ 0\ 0 & -\frac{3l^3}{35} - \frac{x_0 l^2}{5} + \frac{2(L^2 - x_0^2)l}{15}
\end{bmatrix}_{12\times 12}, \quad \text{(A.3)}$$

$$[T_3^e] = \frac{1}{2}\rho a\Omega^2 \begin{bmatrix}
0 & 0 & 0 & 0 & 0 & 0 & 0 & 0 & 0 & 0 & 0 & 0 \\
0 & 0 & 0 & 0 & 0 & 0 & 0 & 0 & 0 & 0 & 0 & 0 \\
0 & 0 & -\frac{12l}{35} - \frac{6x_0}{5} + \frac{6}{5}\frac{L^2 - x_0^2}{l} & 0 & \frac{l^2}{14} + \frac{x_0 l}{5} - \frac{L^2 - x_0^2}{10} & 0 & 0 & 0 & \frac{12l}{35} + \frac{6x_0}{5} - \frac{6}{5}\frac{L^2 - x_0^2}{l} & 0 & -\frac{l^2}{35} - \frac{L^2 - x_0^2}{10} & 0 \\
0 & 0 & 0 & 0 & 0 & 0 & 0 & 0 & 0 & 0 & 0 & 0 \\
0 & 0 & \frac{l^2}{14} + \frac{x_0 l}{5} - \frac{L^2 - x_0^2}{10} & 0 & -\frac{2l^3}{105} + \frac{2(L^2 - x_0^2)l - x_0 l^2}{15} & 0 & 0 & 0 & -\frac{l^2}{14} - \frac{x_0 l}{5} + \frac{L^2 - x_0^2}{10} & 0 & \frac{l^3}{70} + \frac{x_0 l^2 - L^2 l + x_0^2 l}{30} & 0 \\
0 & 0 & 0 & 0 & 0 & 0 & 0 & 0 & 0 & 0 & 0 & 0 \\
0 & 0 & 0 & 0 & 0 & 0 & 0 & 0 & 0 & 0 & 0 & 0 \\
0 & 0 & 0 & 0 & 0 & 0 & 0 & 0 & 0 & 0 & 0 & 0 \\
0 & 0 & \frac{12l}{35} + \frac{6x_0}{5} - \frac{6}{5}\frac{L^2 - x_0^2}{l} & 0 & -\frac{l^2}{14} - \frac{x_0 l}{5} + \frac{L^2 - x_0^2}{10} & 0 & 0 & 0 & -\frac{12l}{35} - \frac{6x_0}{5} + \frac{6}{5}\frac{L^2 - x_0^2}{l} & 0 & \frac{l^2}{35} + \frac{L^2 - x_0^2}{10} & 0 \\
0 & 0 & 0 & 0 & 0 & 0 & 0 & 0 & 0 & 0 & 0 & 0 \\
0 & 0 & -\frac{l^2}{35} - \frac{L^2 - x_0^2}{10} & 0 & \frac{l^3}{70} + \frac{x_0 l^2 - L^2 l + x_0^2 l}{30} & 0 & 0 & 0 & \frac{l^2}{35} + \frac{L^2 - x_0^2}{10} & 0 & -\frac{3l^3}{35} - \frac{x_0 l^2}{5} + \frac{2(L^2 - x_0^2)l}{15} & 0 \\
0 & 0 & 0 & 0 & 0 & 0 & 0 & 0 & 0 & 0 & 0 & 0
\end{bmatrix}_{12\times 12} . \quad \text{(A.4)}$$

In equations (A.1)–(A.4) $\rho$ is the mass density, $a$ is the element cross-sectional area, $l$ is the element length, $\Omega$ is the rotational speed, $L$ is the length of the beam, and $x_0$ is the co-ordinate of the first node in an element. The density and the cross-sectional area are considered constant over the length of an element.

## APPENDIX B: DEFINITION OF ELEMENT MATRICES FOR THREE-DIMENSIONAL SOLID FINITE ELEMENTS

$$[T^e] = \int_{V^e} \rho [N]^{\mathrm{T}} [A_\theta]^{\mathrm{T}} [A_\theta] [N] \, \mathrm{d}V = \int_{-1}^{1} \int_{-1}^{1} \int_{-1}^{1} \rho [N]^{\mathrm{T}} [A_\theta]^{\mathrm{T}} [A_\theta] [N] |J| \, \mathrm{d}r \, \mathrm{d}s \, \mathrm{d}t$$

$$= \rho \sum_{i=1}^{n} w_i \left[ \sum_{j=1}^{n} w_j \left[ \sum_{k=1}^{n} w_k [N]^{\mathrm{T}} [A_\theta]^{\mathrm{T}} [A_\theta] [N] |J| \Big|_{r=r_k} \right] \Big|_{s=s_j} \right] \Big|_{t=t_i}, \tag{B.1}$$

$$[H^e] = \int_{V^e} \rho [N]^{\mathrm{T}} [A_\theta]^{\mathrm{T}} [A] [N] \, \mathrm{d}V = \int_{-1}^{1} \int_{-1}^{1} \int_{-1}^{1} \rho [N]^{\mathrm{T}} [A_\theta]^{\mathrm{T}} [A] [N] |J| \, \mathrm{d}r \, \mathrm{d}s \, \mathrm{d}t$$

$$= \rho \sum_{i=1}^{n} w_i \left[ \sum_{j=1}^{n} w_j \left[ \sum_{k=1}^{n} w_k [N]^{\mathrm{T}} [A_\theta]^{\mathrm{T}} [A] [N] |J| \Big|_{r=r_k} \right] \Big|_{s=s_j} \right] \Big|_{t=t_i}, \tag{B.2}$$

$$[T_2^e] = \frac{1}{2} \int_{V^e} \rho \Omega^2 (L^2 - x^2) \frac{\partial \{S_2\}^{\mathrm{T}}}{\partial x} \frac{\partial \{S_2\}}{\partial x} \, \mathrm{d}V$$

$$= \frac{1}{2} \rho \Omega^2 \int_{-1}^{1} \int_{-1}^{1} \int_{-1}^{1} \left[ L^2 - \left( \sum_{a=1}^{8} N_a x_a \right)^2 \right] \frac{\partial \{S_2\}^{\mathrm{T}}}{\partial x} \frac{\partial \{S_2\}}{\partial x} |J| \, \mathrm{d}r \, \mathrm{d}s \, \mathrm{d}t$$

$$= \frac{1}{2} \rho \Omega^2 \sum_{i=1}^{n} w_i \left[ \sum_{j=1}^{n} w_j \left[ \sum_{k=1}^{n} w_k \left[ L^2 - \left( \sum_{a=1}^{8} N_a x_a \right)^2 \right] \frac{\partial \{S_2\}^{\mathrm{T}}}{\partial x} \frac{\partial \{S_2\}}{\partial x} |J| \Big|_{r=r_k} \right] \Big|_{s=s_j} \right] \Big|_{t=t_i}, \tag{B.3}$$

$$[T_3^e] = \frac{1}{2} \int_{V^e} \rho \Omega^2 (L^2 - x^2) \frac{\partial \{S_3\}^{\mathrm{T}}}{\partial x} \frac{\partial \{S_3\}}{\partial x} \, \mathrm{d}V$$

$$= \frac{1}{2} \rho \Omega^2 \int_{-1}^{1} \int_{-1}^{1} \int_{-1}^{1} \left[ L^2 - \left( \sum_{a=1}^{8} N_a x_a \right)^2 \right] \frac{\partial \{S_3\}^{\mathrm{T}}}{\partial x} \frac{\partial \{S_3\}}{\partial x} |J| \, \mathrm{d}r \, \mathrm{d}s \, \mathrm{d}t$$

$$= \frac{1}{2} \rho \Omega^2 \sum_{i=1}^{n} w_i \left[ \sum_{j=1}^{n} w_j \left[ \sum_{k=1}^{n} w_k \left[ L^2 - \left( \sum_{a=1}^{8} N_a x_a \right)^2 \right] \frac{\partial \{S_3\}^{\mathrm{T}}}{\partial x} \frac{\partial \{S_3\}}{\partial x} |J| \Big|_{r=r_k} \right] \Big|_{s=s_j} \right] \Big|_{t=t_i}, \tag{B.4}$$

where $w_i$, $w_j$, $w_k$ are the weight factors for the integration, $|J|$ is the determinant of the Jacobian matrix, and $r_k$, $s_j$, $t_i$ are the dimensionless co-ordinates of the Gaussian integration points. The density is considered constant over the volume of an element.